OPTICAL TRANSITION RADIATION INTERFEROMETRY FOR THE A0 PHOTOINJECTOR*

G. Kazakevich#, BINP SB RAS, Novosibirsk, Russia
H. Edwards, R. Fliller, S. Nagaitsev, J. Ruan, R. Thurman-Keup (Fermilab, Batavia, Illinois) U.S.A.

Abstract

Optical Transition Radiation Interferometry (OTRI) is a promising diagnostic technique and has been successfully developed and used for investigation of relativistic beams. For mid-energy accelerators the technique is traditionally based on thin polymer films (the first one is being transparent for visible light), which causes beam multiple scattering of about 1 mrad. A disadvantage of those films is unacceptable vacuum properties for photoinjectors and accelerators using superconducting cavities. We have studied the application of thin mica sheets for the OTRI diagnostics at the A0 Photoinjector in comparison with 2.5 μm thick Mylar films. This diagnostic is also applicable for the ILCTA-NML accelerator test facility that is planned at Fermilab. This report discus the experimental setups of the OTR interferometer for the A0 Photoinjector and presents comparisons of simulations and measurements obtained using Mylar and mica-based interferometers.

INTRODUCTION

A relativistic charged particle passing through the interface of two media having different permittivities generates Transition Radiation (TR), [1], with a significant portion in the optical range. This Optical Transition Radiation (OTR) is widely used for transverse beam size monitoring. Moreover, OTR contains information about the energy, energy spread and divergence of the beam. Using the interference of the OTR from two thin films [2] inserted in the beam trajectory one can measure the beam parameters. Application of OTR Interferometry (OTRI method) to mid-energy photoinjectors requires transparency of one of the films and minimum thickness of the first one. The method employing thin polymer films for mid-energy accelerators has been described in a number of works, [3-5], demonstrating good agreement between measurements and calculations. In this paper we consider application of this method for cold mid-energy beams using both, traditional polymer films in the interferometer, and non-traditional films with better vacuum properties.

OTRI SETUP WITH 45° INCIDENCE FOR A0 FACILITY

The traditional setup for OTR interferometry (OTRI) at the A0 Photoinjector employs two thin films, displaced by a distance *D* along the beam trajectory and mounted in the accelerator beamline. The first film is optically transparent while the second one has a mirrored metal coating. We studied properties of this setup for interferometers based on 2.5 μm thick Mylar and 6 μm thick Ladd Research mica sheets. Although mica is a birefringent crystal having different refractive indices in the plane of cleavage, the difference between the indices is small enough, [6], thus one obtains a clear interpretation of the fringes for quite thin mica sheets.

The OTRI patterns were obtained using the relay optics of Fig. 1.

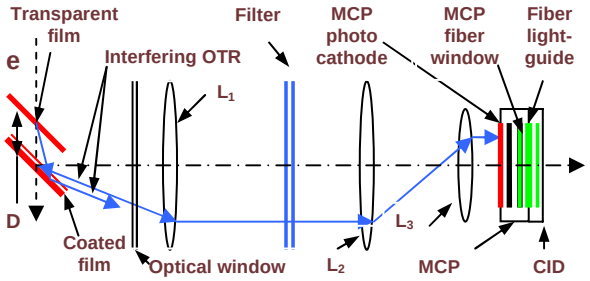

Fig. 1. The 45° incidence OTRI setup.

The OTR interferometer was mounted inside a 6-way beamline cross in the focal plane of lens L_1. The objective L_2-L_3 is combined in a telescope, matching the fringe size to the photodetector area. Focal lengths and locations of the lenses were chosen to minimize distortion of the OTRI pattern caused by the beam size. Thus the distance L_1-L_2 is equal to f_1+f_2 and the distance L_3-*MCP photocathode* is equal to f_3, where f_1, f_2, f_3 are the focal lengths for lenses L_1, L_2 and L_3, respectively. So the relay optics matrix elements M_{ij} are:

$$M_{11}=M_{22}=0,\ M_{12}=\frac{-f_1\cdot f_3}{f_2},\ M_{21}=\frac{f_2}{f_1\cdot f_3}.$$

To prevent beam dark current from blurring the fringes we used a gated Intensified CID (ICID) camera based on a Hamamatsu MCP intensifier with 60 ns-duration gating pulses. The images of the OTRI pattern for 16 MeV electrons at the energy spread of ~70 keV obtained with Mylar and mica-based interferometers are given in Fig. 2.

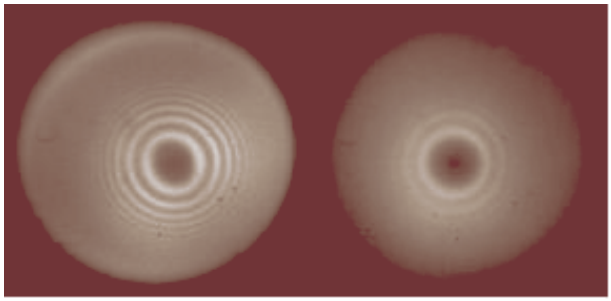

Fig. 2. The fringes obtained at 45° incidence setup with Mylar (left) and mica (right) -based interferometers.

* This manuscript has been authored by Fermi Research Alliance, LLC under Contract No. DE-AC02-07CH11359 with the U.S. Department of Energy.
#kazakevi@fnal.gov

The OTRI images were obtained using a 40 nm wide bandpass filter with a central wavelength of 450 nm. The distance *D* values were chosen to be 0.85 mm and 0.707 mm for Mylar and mica -based interferometers, respectively.

We calibrated the existing optical setup on an optical bench replacing the interferometer with a 50 μm-diameter pinhole and measuring the diffraction pattern from a He-Ne laser. The measurements showed that the existing ICID photodetector has poor fringe visibility because of blurring presumably due to an inherent misalignment between the MCP fiber optic output window and the CID camera fiber optic input window. Comparison of the computed pinhole diffraction pattern with the measured one showed that the ICID photodetector has a resolution in the images of ≈4 pixels that corresponds to an angular photodetector resolution of ≈2.1 mrad. Thus we convolved the computed OTRI patterns over measured angles with $\sigma_{meas.}$ =2.1 mrad. Additional distortions in the intensified photodetector are caused by nonlinearities of the MCP intensifier at high signal. That results in some systematic errors of the fringe visibility. We have made an estimate of the nonlinearity on the optical bench by comparing the measured pinhole diffraction pattern with the computed one. This estimate was used to provide a rough correction to the measured OTRI profiles.

To determine the beam divergence at the interferometer location we have measured the beam r.m.s. sizes, $\sigma_b(x)$, along the beamline at the gun solenoid current that produces a waist at the entrance to the beamline. The measured beam sizes include a space charge effect during flight of the beam along the beamline. Using the slits technique, the r.m.s. beam divergence, $\theta_b(0)$, has been measured at the beamline entrance. Focusing the beam by a quad upstream of the interferometer, we measured the beam r.m.s. size, $\sigma_{bf}(L)$, at the interferometer position. Then the r.m.s. beam divergence at the interferometer position, $\theta_{bf}(L)$, was determined as:

$$\theta_{bf}(L) = \left(\sqrt{\theta_b{}^2(0) + \left(\frac{\sigma_b(L) - \sigma_b(0)}{L} \right)^2} \right) \cdot \frac{\sigma_b(L)}{\sigma_{bf}(L)},$$

where *L* is distance from the beamline entrance to the interferometer position, index *f* points to focusing by the quad. In Figure 3 are plotted the measured $\sigma_b(x)$ values for 16 MeV beam with bunch charge of 1 nC at a measured energy spread of approximately 70 keV.

The computed profiles include the beam angles, angles of the multiple scattering for the Mylar and the mica-based interferometers, the beam energy spread, the filter spectral bandwidth, [7], and the ICID photodetector resolution measured with the pinhole. The measured pattern profiles were corrected for the MCP nonlinearity.

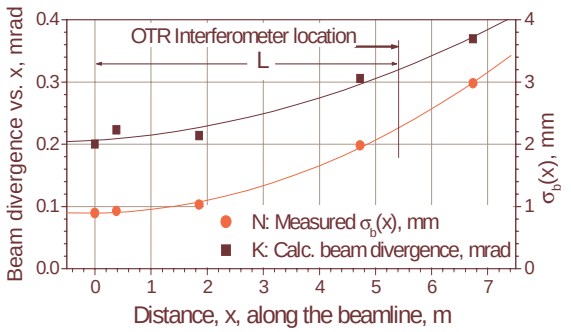

Fig. 3. Points N show measured $\sigma_b(x)$ along the beam line for 16 MeV, 1 nC bunches (right scale). Points K show beam divergence values calculated from measured $\sigma_b(x)$ data along the beamline (left scale).

The measured fringe profiles for the 45° beam incidence OTRI setup at the $\sigma_{meas.}$=2.1 mrad, the σ_b=1.2 mrad, and the σ_E≈70 keV are plotted in Figure 4.

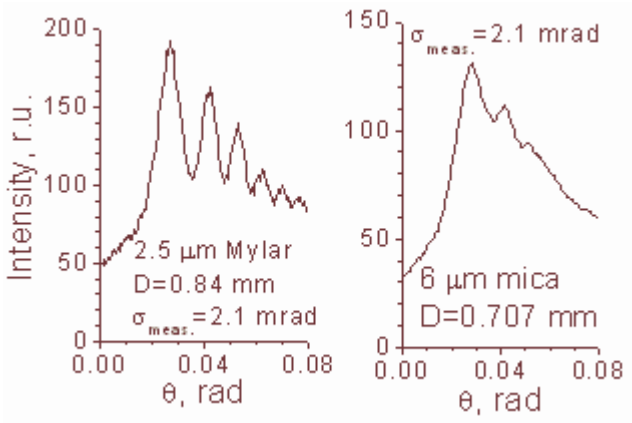

Fig. 4. Fringe profiles obtained with Mylar-based (left) and mica-based (right) OTRI setup at 45° incidence and 16 MeV electrons and σ_b=1.2 mrad.

The right plot demonstrates applicability of the mica-based interferometers for the OTRI techniques, but points to necessity in a decrease the first mica thickness to decrease the contribution caused by multiple scattering. Simple realization of that for experiments intended to determine the beam divergence was studied with a setup employing normal incidence of electrons in the OTR interferometer.

OTRI SETUP WITH NORMAL INCIDENCE

Optical bench measurements showed better visibility of the pinhole diffraction pattern when using a separate MCP intensifier with an ordinary CCD camera plus objective focused on the output window of the intensifier.

This improvement of the photodetector was realized in the setup with normal incidence of the electron beam, Figure 5.

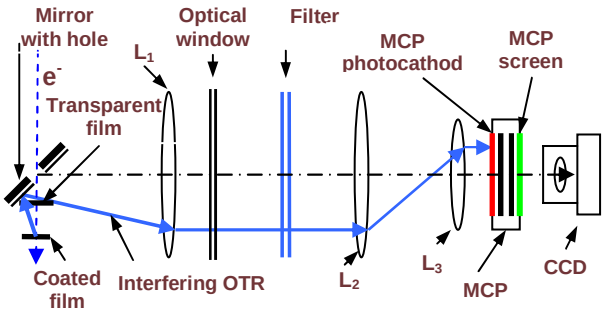

Fig. 5. The OTRI setup with normal incidence of the electron beam. The mirror surface was inclined to the beam trajectory with angle of 45°.

The OTR interferometer, the mirror with 5 mm-diameter hole for passing electrons), and the collimating lens L_1 were mounted in two 6-way beamline crosses. In the upstream one were mounted the mirror and the lens L_1. The interferometer was located in the downstream (second one) cross. The OTRI pattern light was transmitted through the L_1 lens, the vacuum optical window, the bandpass filter, and through the L_2-L_3 objective to the gated MCP intensifier. The intensified pattern was detected by the CCD camera with an ordinary objective. The resolution of the combined photodetector, as measured on the optical bench, is ~0.9 mrad. This was convolved with the computed fringe profiles. The normal incidence setup and the CCD-based readout allowed a significant improvement in the fringe visibility for both Mylar and mica-based interferometers. The corresponding fringe profiles measured for different beam divergence, σ_b, are plotted in Figures 6 for the Mylar and mica –based interferometers, respectively.

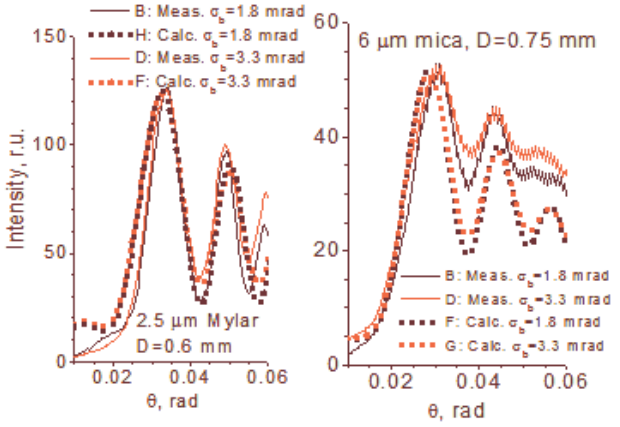

Fig. 6. Measured (solid lines) and computed (dots) fringes for the Mylar (left) and mica (right) -based interferometers at normal incidence, beam energy of 16 MeV, σ_E~100 keV and $\sigma_{meas.}$=0.9 mrad.

The computed interference patterns include the multiple scattering of the electrons, beam energy spread, angles in the beam, the filter spectral bandwidth, [7], and resolution of the combined photodetector. The measured fringes were corrected for the MCP nonlinearity. We do not consider here some additional blurring caused by imperfections of the milled mirror in visible light.

The Figure 6 plots show a few percent difference in visibility for computations and measurements with the Mylar-based interferometer at the beam divergence of ≥ 1.8 mrad. With 6 μm mica-based interferometer the difference is few tens of percent because of strong multiple scattering in relatively thick mica sheet. Decreasing the mica thickness will allow improvements in the mica-based interferometers.

A comparison of the results obtained with both the 45° and normal incidence setups shows that the latter is more preferable because of the smaller effective thickness of the first film than for 45° incidence, especially if one considers lower angles in the beam. Moreover the optical readout of the intensified fringes used in the last setup provides lower blurring due to better image resolution. That gives better visibility of the fringes allowing better determination of lower angles in the beam.

Note that the described setup with normal incidence was mounted in the standard beamline elements (6-way crosses) with an aperture of ≈ 47 mm, so the lens L_1 had limited size (the L_1 diameter is of 38 mm at f_1≈200 mm). Because of that aperture the range of the fringe observation angles was limited to <80 mrad. Moreover, the central part of the range is missed due to the hole in the mirror, so the real detection range was about ± (13-65) mrad, and as such we are able to observe only a few fringes at low order. Some distortion of the measured fringes in comparison with computed shows that it is preferable to increase the L_1 aperture and to decrease the hole diameter in the mirror. However the obtained interference patterns allowed us to determine the visibility as a function of the beam divergence at normal operating conditions of the A0 Photoinjector.

CONCLUSION

The results obtained with the normal incidence setup allow us to determine the beam divergence in the range of about 1-8 mrad for Mylar–based interferometer at A0 Photoinjector. A thickness of the mica sheets of ~ 3 μm will result in approximately same range of sensitivity while providing good vacuum properties of the apparatus.

REFERENCES

[1] V.L Ginzburg and I.M. Frank, J. Exp. and Theoret. Phys., Vol. 16, pp. 15-21, 1946.
[2] L. Wartski et al., J. of Appl. Phys. Vol. 46, No. 8, 3644-3653, 1975.
[3] R.B. Fiorito and D.W. Rule, AIP Conference Proceed. Beam Instrumentation Workshop, V. 319, pp. 21-37, 1994.
[4] R.B. Fiorito and A.G. Shkvarunets, Proceedings DIPAC 2003, pp. 89-91, 2003.
[5] D.W. Rule et. al., NIM A296, (1990), 739-743,
[6] E. Hecht and A Zajac, Optics, Addison-Wesley, 1979
[7] G. Kazakevich at al., FERMILAB-PUB-07-055-AD